Artificial Cells

How to cite: *Angew. Chem. Int. Ed.* **2023,** *62,* e202216966
International Edition: doi.org/10.1002/anie.202216966
German Edition: doi.org/10.1002/ange.202216966

Confining the Sol-Gel Reaction at the Water/Oil Interface: Creating Compartmentalized Enzymatic Nano-Organelles for Artificial Cells

Jenifer Pendiuk Gonçalves, Duangkamol Promlok, Tsvetomir Ivanov, Shijia Tao, Timo Rheinberger, Seong-Min Jo, Yingjie Yu, Robert Graf, Manfred Wagner, Daniel Crespy, Frederik R. Wurm, Lucas Caire da Silva, Shuai Jiang, and Katharina Landfester**

Abstract: Living organisms compartmentalize their catalytic reactions in membranes for increased efficiency and selectivity. To mimic the organelles of eukaryotic cells, we develop a mild approach for in situ encapsulating enzymes in aqueous-core silica nanocapsules. In order to confine the sol-gel reaction at the water/oil interface of miniemulsion, we introduce an aminosilane to the silica precursors, which serves as both catalyst and an amphiphilic anchor that electrostatically assembles with negatively charged hydrolyzed alkoxysilanes at the interface. The semi-permeable shell protects enzymes from proteolytic attack, and allows the transport of reactants and products. The enzyme-carrying nanocapsules, as synthetic nano-organelles, are able to perform cascade reactions when enveloped in a polymer vesicle, mimicking the hierarchically compartmentalized reactions in eukaryotic cells. This in situ encapsulation approach provides a versatile platform for the delivery of biomacromolecules.

Introduction

Compartmentalization is a key feature of life because it enables spatiotemporal control over multi-step biological reactions and metabolic processes in living cells. Cellular and subcellular compartments (organelles) provide a confined environment that increases the efficiency and selectivity for enzymatic reactions and separates different biological processes.[1] In an attempt to decode the rules of life and develop micro-machines with clinical and industrial value, researchers have been trying to artificially reproduce the compartmentalization of biological processes found in nature by using bottom-up strategies to create synthetic cell analogues.[2] To this purpose, various micro and nanocontainers (e.g., a myriad of polymer vesicles and capsules, liposomes, virus-like particles, inorganic cages, and even enzyme-templated nanocapsules)[3] have been developed and combined to form multi-compartmentalized vesicles.[4] Nevertheless, challenges remain for efficient and safe enzyme encapsulation such as difficulty in loading enzymes to pre-formed compartments, control of shell permeability, and structure instability upon environmental changes.[3]

Hollow silica nanocontainers are valuable biomimetic encapsulation systems due to their married merits of a capsular configuration (i.e., large internal cargo-reservoir cavity surrounded by a semipermeable shell that provides protection and selective permeability) with the mechanical robustness, porosity, and versatile chemistry of the silica materials.[5] Although low molecular weight drugs can be post-loaded into preformed hollow capsules, the macromolecular nature of enzymes hinders their diffusion across the silica shell to the interior.[6] Therefore, in situ compartmentalization would be the ideal approach for enzymes.[6a] Nevertheless, hollow silica nanostructures are typically formed by using etching or template-mediated approaches[7] that require the removal of template particles and surfactants by thermal calcination, hydrothermal treatment, or solvent extraction, which are deleterious for the sensitive

[*] Dr. J. P. Gonçalves, D. Promlok, T. Ivanov, T. Rheinberger, S.-M. Jo, R. Graf, M. Wagner, F. R. Wurm, Dr. L. Caire da Silva, Prof. K. Landfester
Max Planck Institute for Polymer Research, Ackermannweg 10, 55128 Mainz (Germany)
E-mail: landfester@mpip-mainz.mpg.de
Dr. J. P. Gonçalves
Federal University of Paraná
Av. Cel Francisco H dos Santos, s/n, CEP 81530-980, Curitiba-PR (Brazil)
Assoc. Prof. D. Crespy
Department of Materials Science and Engineering, School of Molecular Science and Engineering, Vidyasirimedhi Institute of Science and Technology (VISTEC)
Rayong 21210 (Thailand)
S. Tao, Y. Yu, Prof. S. Jiang
Key Laboratory of Marine Drugs, Chinese Ministry of Education, School of Medicine and Pharmacy, Ocean University of China
Qingdao 266003 (China)
E-mail: jiangshuai@ouc.edu.cn

enzyme molecules.[8] Alternatively, hollow silica nanocapsules can be produced without template particles or surfactants by using a modified amphiphilic precursor that self-assembles as vesicles around the water-dissolved enzymes. However, this process results in enzyme encapsulation efficiency of lower than 50 % and requires basic ammonia solution as a catalyst,[9] which is deleterious for enzyme activity.[10]

Considering that, herein we developed a universal approach for the straightforward synthesis of aqueous-core mesoporous-shell silica nanocapsules (AMSNs) that allows an in situ, safe, and defined encapsulation of enzymes, mimicking the functions of natural eukaryotic organelles and perform complex biological reaction cascades. The AMSNs were synthesized via an interface-confined sol-gel process in an inverse (water-in-oil) miniemulsion. The AMSNs have a large internal cavity to store the enzymes and a semipermeable shell to keep the enzymes trapped while allowing the diffusion of reaction substrates and products. The challenge of restricting the sol-gel reactions to the water-oil interface without using harsh conditions (i.e., ammonia as catalyst, CTAC as templating agent, and ethanol for surfactant extraction)[11] has been overcome by simply introducing an amine-containing trialkoxysilane as a comonomer for common tetraalkoxysilanes during the silica formation. As outlined in the left part of Figure 1, the successful formation of a silica shell around the nanodroplets can be achieved under neutral pH conditions and without using templating agents. Enzymes can be efficiently encapsulated in the semipermeable AMSNs, which can successfully perform enzymatic reactions individually, as well as be further used as nano-organelles to construct artificial cells (right part of Figure 1). Furthermore, this strategy allows controlling the enzyme distribution and the resulting functionalities and reactions of integrated multi-organelle systems.

Results and Discussion

In the first part of this study, we encapsulated enzymes inside the AMSNs by using an inverse (water-in-oil) miniemulsion process. The enzymes were first dissolved in water, which was emulsified to form nanodroplets in a cyclohexane continuous phase. Afterward, silica precursors were added in order to form a core–shell structure containing internally dissolved enzymes. Indeed, the key challenge is an efficient confinement of silica formation at the oil-water interface, in the absence of any templating particles, cationic surfactants or strong acid and base as the catalysts. This is due to the fact that upon contact with the water phase, alkoxysilanes are hydrolyzed, become hydrophilic due to silanol groups, and therefore diffuse into the aqueous droplets to form solid nanoparticles upon secondary nucleation. To overcome this challenge, we introduced here a second precursor, an amine-containing trialkoxysilane (APTES), which features an amphiphilic nature that shows a preferential interfacial accumulation.[12] Moreover, the amino group of APTES can catalyze the silica hydrolysis and condensation locally in order to accelerate the silica formation at the interface. Therefore, after a systematic investigation, we were able to control the silica condensation uniquely at the interface based on the mechanism of controlled hydrolysis kinetics and electrostatic interactions between tetraalkoxysilanes and APTES.

We performed a systematic study to investigate the critical roles of APTES for the interfacial confinement of silica condensation. First, we varied the ratio of APTES to the comonomer tetramethoxysilane (TMOS) (or tetraethoxysilane, TEOS) (Table S1). Second, we investigated the effect of the pH value of the aqueous phase (adjusted using different concentrations of ammonia) on the condensation by correlating the composition of silica precursors with the morphology of resulting nanostructures (Figure 2).

From this morphological study, we found some important information. First, the use of TMOS or TEOS (Figure 2a1–a5, S1), or APTES alone (Figure 2e1–e5) in the

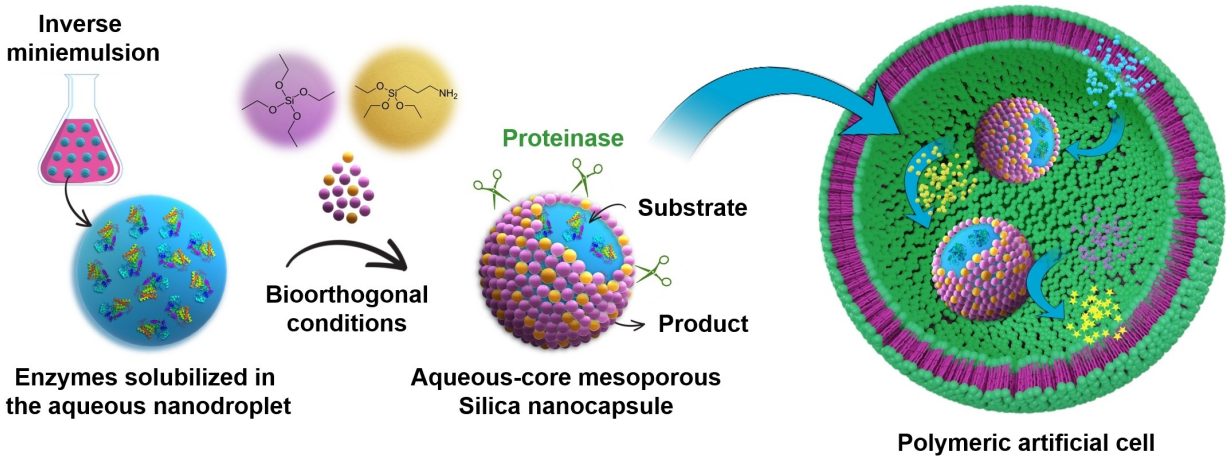

Figure 1. Schematic illustration of the interface-confined silica co-condensation process in an inverse miniemulsion for the bioorthogonal synthesis of AMSNs as nanocontainers for enzymes (left) and their application as nano-organelles in artificial cell systems (right).

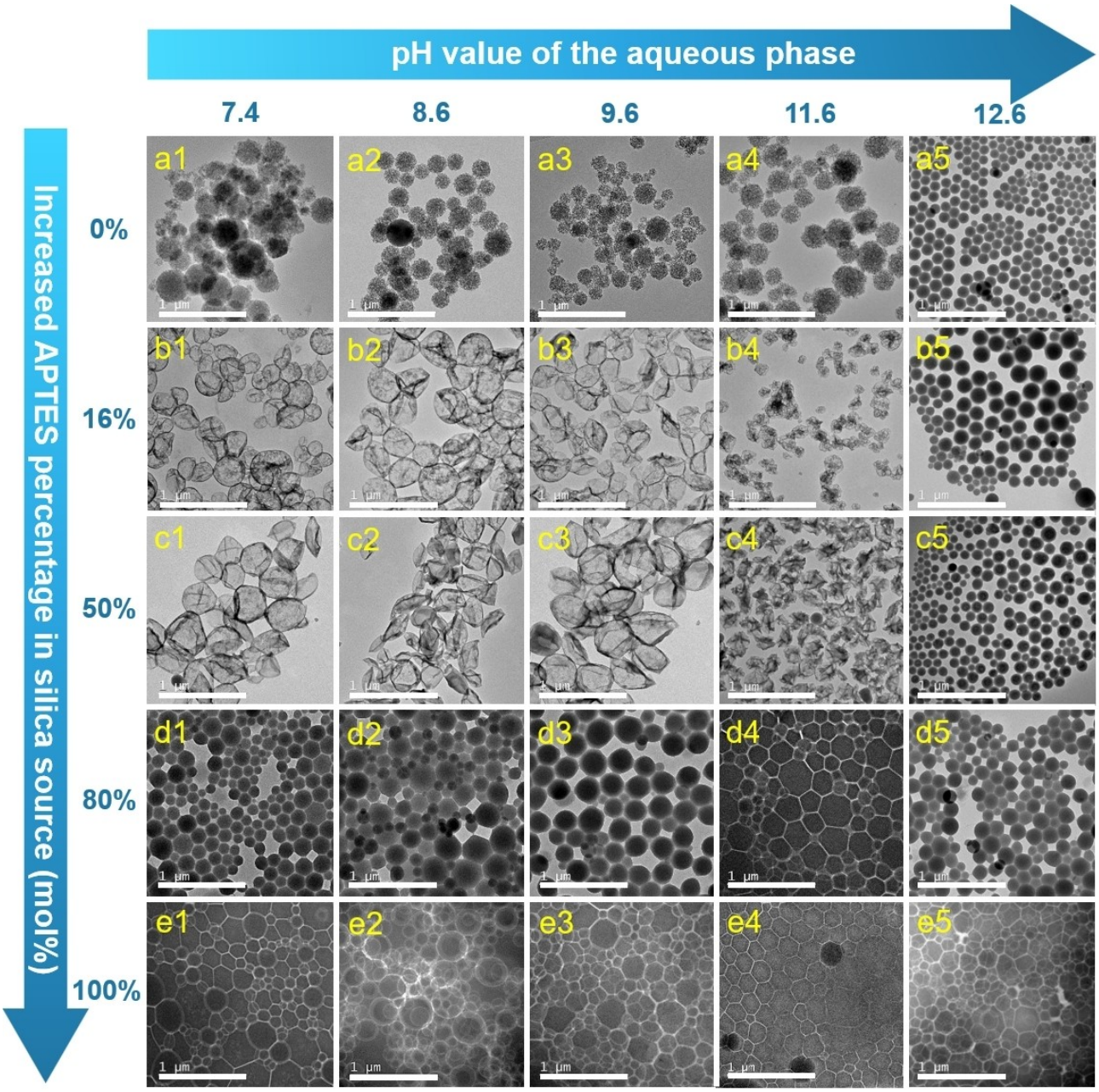

Figure 2. Correlation between APTES:TMOS molar ratio in the precursor mixture and variations in the aqueous phase pH value with the morphology of resulting nanostructures characterized by TEM. APTES molar percentage in the precursors increases from top to bottom. The pH value of the aqueous phase of the miniemulsion increases from left to right. Scale bars = 1 µm.

silica source generates only nanoparticles. However, the use of 16 or 50 mol % APTES mixed with TMOS results in core–shell capsules (Figure 2b1, c1), confirming the essential role of APTES for the interfacial confinement of the co-condensation. Further confirmation of the production of solid versus core–shell nanoparticles was obtained by scanning electron microscopy (SEM) (Figures S2 and S3). In the case of TEOS as comonomer, core–shell capsules are formed only at 16 % APTES, while 50 % APTES produces solid particles (Figure S1). Taken together, these results show that both the choice of tetraalkoxysilane and its ratio to APTES are crucial for the interfacial condensation. Second, when precursors are used separately (Figure 2a, e), the basic pH value, which accelerates the sol-gel process, does not lead to the formation of a core–shell structure by itself. In the case of 16 and 50 mol % APTES in the mixtures, core–shell capsules are formed at the pH range from 7.4 to 11.6 (Figure 2b1–b4, c1–c4), while only solid particles are observed when the pH value is increased to 12.6 (Figure 2b5, c5), indicating that such high pH value actually does not favor the interfacial co-condensation. The pH does not have an effect on the particle size (Figure S4).

This systematic study showed that AMSNs can be successfully produced under a physiological pH condition (i.e., pH 7.4, Figure 2b1, c1), which is ideal for maintaining the structure and activity of most enzymes to be encapsulated.

To explore in greater depth the above observations, we first studied the composition of the resulting nanocapsules (presented in Figure 2b1–b5, c1) by using ^{29}Si MAS NMR spectroscopy after purification to remove unreacted silica precursors. Results show that both APTES and TMOS are indeed incorporated in the silica network (Figure S5). No T_1 and Q_1 signals are detected, showing the high condensation degrees of both precursors. The ratios between APTES and TMOS that were added to the synthesis and the ratios measured in the final nanocapsules are very similar (Table 1), showing their equal incorporation during the interfacial co-condensation process.

We hypothesized that the positive charge, amphiphilicity and catalytic features of APTES, combined with a fast hydrolysis kinetic of the comonomer TMOS are the key factors for an efficient interfacial co-condensation (Figure 3A). The amino group of APTES has a pK_a value of about 10–10.8.[13] At lower pH values, APTES is positively charged (APTES$^+$) due to protonation of the amino group, which increases its hydrophilicity; in contrast to its three ethoxy groups that are more hydrophobic. Therefore, APTES$^+$ behaves as an amphiphile at the oil-water interface prior to hydrolysis of the ethoxy groups. Upon hydrolysis, the ethoxy groups are converted to hydrophilic silanol groups. The hydrolyzed APTES$^+$ molecules become more hydrophilic and tend to diffuse into the water droplet,[12] explaining why only solid nanoparticles are obtained when APTES is used alone (Figure 2e). On the other hand, the comonomer TMOS hydrolyses rapidly after contact with water. The formed silanol groups have a pK_a value about 4–7,[14] meaning that the hydrolyzed TMOS molecules are negatively charged under our experimental conditions (i.e., pH 7.4–12.6). When a pair of APTES and TMOS is applied, electrostatic interactions might take place between APTES$^+$ and hydrolyzed TMOS at the water-oil interface.

To confirm the hypothesis that an electrostatic interaction enabled the assembly between APTES and TMOS at the interface, we used the cationic surfactant cetyltrimethylammonium chloride (CTAC) to replace APTES in the protocol since it has a long alkyl chain with a positive charge derived from the quaternary ammonium. Indeed, CTAC can efficiently confine the silica condensation at the interface to form core–shell nanocapsules, starting at a molar proportion of 2 mol % compared to the amount of TMOS at pH 11.6 (Figure 3B a). Although CTAC proved to be efficient for the AMSNs production, it is important to mention that it strongly interacts with proteins even at low concentrations, leading to their denaturation and aggregation,[15] which makes such an approach unfeasible for the encapsulation of biomacromolecules. Exposure to CTAC, and other chemicals such as ammonia or ethanol, that are often used for forming silica nanomaterials, drastically reduced the enzyme activity (Figure S6).

The amino group of APTES can also catalyze the hydrolysis and condensation of alkoxysilanes by locally increasing the pH value.[16] To understand this phenomenon in our model, we studied the hydrolysis kinetics of individual silica precursors (APTES, TMOS, and TEOS) and their combinations by ^{1}H NMR spectroscopy. TEOS shows very slow hydrolysis at pH 7.4, with no hydrolysis observed for over 20 h (Figure S7). In comparison, TMOS hydrolyzes relatively fast (Figure 3C), with a half-life ($t_{1/2}$) of 4.4 h, due to its shorter alkoxy groups that lead to a faster nucleophilic hydrolytic reaction.[17] APTES also shows fast hydrolysis ($t_{1/2}$ = 6.3 h, Figure 3C) compared with TEOS due to the catalytic effect of the amino groups.[18] Corroborating this idea, compound n-propyltrimethoxysilane (which has a similar structure as APTES, but does not contain -NH_2), used in a control experiment, does not show any hydrolysis after 3 h (Figure S8). Furthermore, adding APTES to the tetraalkoxysilanes accelerated the hydrolysis of both TMOS, with its $t_{1/2}$ decreasing from 4.4 h (used alone) to 0.8 h (Figure 3C), and TEOS (Figure S9). Finally, in the morphological study, replacing APTES with organosilanes that have a similar structure but do not contain amino groups leads to formation of nanoparticles (Figure S10) instead of core–shell nanocapsules (Figure 2b1).

Although APTES catalyzes the hydrolysis of alkoxysilanes, the intrinsic hydrolysis rate and water-solubility of the comonomers are critical for an efficient interfacial co-condensation process. This explains our observation that, at 50 mol % APTES in the precursors, TMOS results in nanocapsules (Figure 3D b) while only nanoparticles are obtained by using TEOS (Figure 3D d). Due to lower water-solubility and slower hydrolysis kinetics, only part of the TEOS molecules hydrolyzed in a short time and available at the interface for the co-condensation with APTES. Therefore, the incorporated TEOS amount (51 % TEOS:49 % APTES measured by ^{29}Si NMR; Table S2 and Figure S11) is much lower than the added concentration (84 % TEOS:16 %

Table 1: Contents of $Q_{(n)}$ and $T_{(n)}$ sites in different samples obtained from ^{29}Si MAS NMR spectroscopy through deconvolution of the spectra. Samples were washed twice with cyclohexane and then freeze-dried before ^{29}Si MAS NMR measurement. $T_2 \approx 60$ ppm, $T_3 \approx 70$ ppm, $Q_2 \approx 90$ ppm, $Q_3 \approx 100$ ppm, $Q_4 \approx 110$ ppm.

Corresponding sample in Figure 2	% of APTES added to the synthesis	pH of water phase	T_2 [%]	T_3 [%]	Q_2 [%]	Q_3 [%]	Q_4 [%]	% of APTES incorporated (T2 + T3)
b1	16	7.4	9	11	3	42	35	20
b2	16	8.6	5	13	7	32	43	18
b3	16	9.6	7	9	8	31	45	16

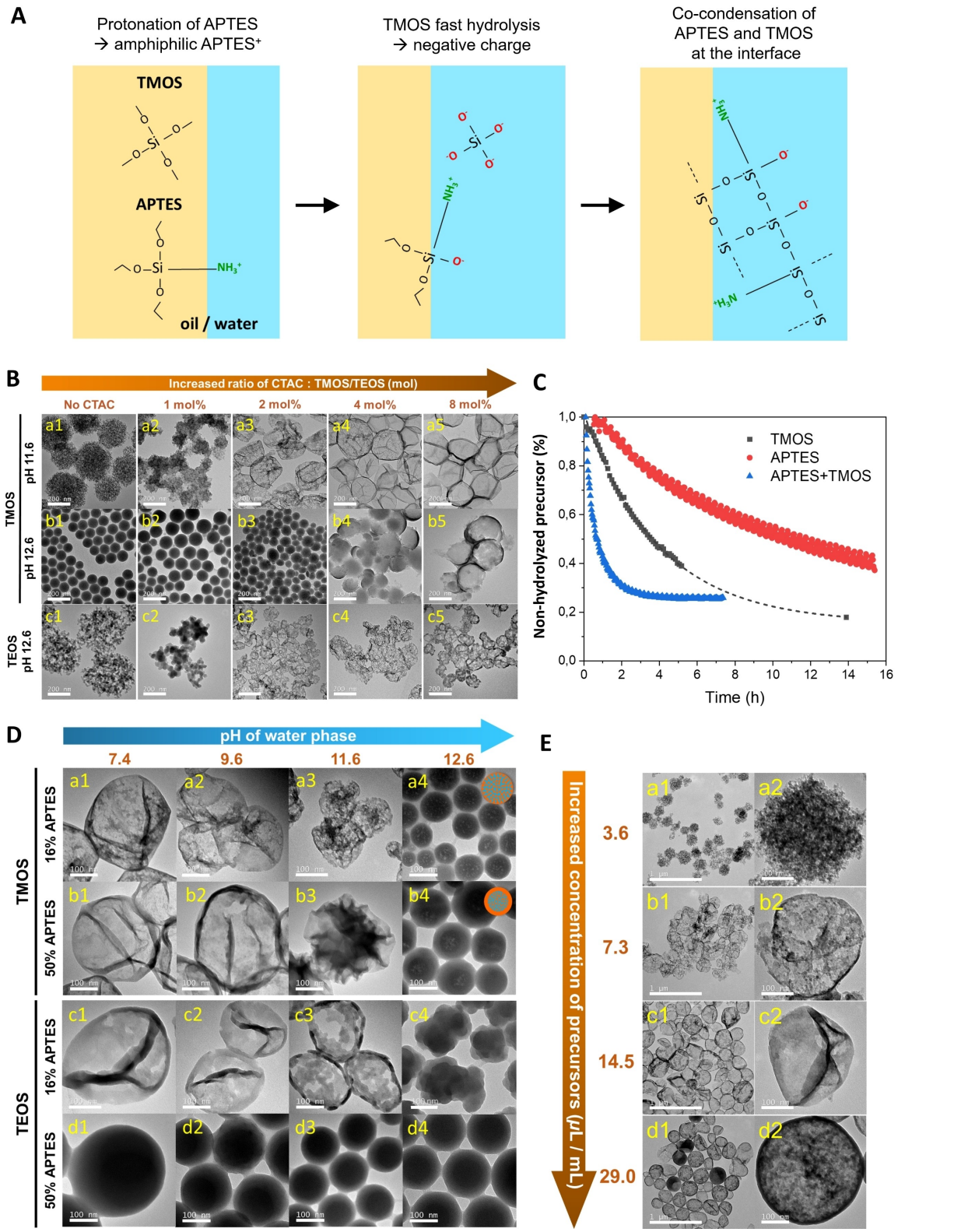

Figure 3. A) Schematic illustration of interfacial silica co-condensation mechanism that results in the formation of core–shell nanocapsules in inverse (water-in-oil) miniemulsion. B) The correlation between the concentration of cationic surfactant CTAC and the morphology of resulting nanoparticles by using TMOS or TEOS as the silica source. Scale bars = 200 nm. C) Hydrolysis kinetics of silica precursors: APTES, TMOS and their combination (16 mol% APTES:84 mol% TMOS). D) The correlation between the APTES:TMOS/TEOS molar ratio in silica source and the morphology of resulting nanoparticles characterized by high resolution TEM. Scale bars = 100 nm. E) The morphology of nanoparticles prepared by using varied concentrations of silica precursors in the emulsion: (a1, a2) 3.6 μL mL^{-1}, (b1, b2) 7.3 μL mL^{-1}, (c1, c2) 14.5 μL mL^{-1}, and (d1, d2) 29.0 μL mL^{-1}. The percentage of APTES in silica source (APTES + TMOS) is 16 mol%. Scale bars in left images = 1 μm, in right images = 100 nm.

APTES). As a consequence, an increase in the APTES ratio in this case leads to precursor migration into the water phase and the formation of solid particles (Figure 3D d). In comparison, TMOS, which has faster hydrolysis than TEOS, results in core–shell nanocapsules (Figure 3D b). Therefore, fast hydrolysis of the co-precursor is crucial for the co-condensation with APTES at the interface.

Additionally, the total amount of silica precursors added to the synthesis is also important. As shown in Figure 3E, core–shell structures are formed above the concentration of 7.3 μL of the precursor mixture (16 mol % APTES:84 mol % TMOS) per mL of emulsion. Below that, nanoparticles are obtained likely because there are insufficient precursor molecules at the interface to form a connected silica network in a short time, before the agglomerates of condensed silica migrate into the water phase due to the increased hydrophilicity of $APTES^+$. Calculations [using Equation (1)–(4) in the Supporting Information] show that the use of 14.5 μL of precursor per mL of emulsion results in feeding densities of APTES and TMOS on the droplet surface of 13 and 68 molecules nm^{-2}, respectively. According to an estimation [using Equation (5) in the Supporting Information], these feeding densities should lead to the formation of a 4.2 nm thick silica layer, assuming 100 % conversion and that the density of the silica layer corresponds to bulk silica density (2.2 $g\,cm^{-3}$). Such theoretical value is identical to the shell thickness (ca. 4 nm) measured from the transmission electron microscopy (TEM) image in Figure 2b1.

The aqueous phase pH value was also further studied for understanding the interfacial confinement of silica condensation. In addition to 16 or 50 mol % APTES leading to the formation of nanocapsules in the pH range of 7.4 to 11.6 (Figure 2b and c), their shells look thinner as the pH value increases. At pH 11.6, collapsed nanocapsules with very thin shell are observed upon drying (Figure 2b4 and 3D a3). Remarkably, only solid nanoparticles are obtained at pH 12.6 regardless of the APTES ratio (Figure 2b5, c5). By using high resolution TEM, we found that these nanoparticles actually have a core–shell structure composed of a porous core surrounded by a solid shell (Figure 3D a4, b4). This inhibited interfacial confinement effect at pH 12.6 was attributed to two possible reasons. 1) Within the pH range of 7.4 to 11.6, the alkoxysilane condensation is faster than the hydrolysis. Above pH 10, the condensation rate starts to decrease while the hydrolysis rate continuously increases with the pH value.[19] At pH 12.6, the hydrolysis rate surpasses condensation, which leads to the migration of hydrolyzed precursors into the aqueous phase. 2) The electrostatic confinement of the reaction depends on APTES positive charge. At pH 12.6, the amino group of APTES is deprotonated as neutral $-NH_2$, which inhibits its interaction with hydrolyzed TMOS for keeping the assembly at the interface.

In the previously described systematic study, ammonia (which is also a catalyst for the silica sol-gel process) was used in the aqueous phase of the miniemulsion to intentionally vary its pH value in order to understand the role of the amino group from APTES. In this section, by understanding that our synthetic approach is based on the electrostatic interaction between hydrolyzed TMOS and APTES, that APTES itself can act as a local catalyst for the reaction, and that a neutral pH is highly desirable in contact with enzymes, we show that AMSNs can finally be directly prepared by using ultrapure water (pH 7.0) or PBS (pH 7.4) as aqueous phases (Figure 4).

As a proof-of-concept study, we used horseradish peroxidase (HRP) and glucose oxidase (GOD) as model enzymes to prove that they could be safely encapsulated in AMSNs under mild conditions. As outlined in Figure 5A, the idea of encapsulating enzymes in AMSNs through a bioorthogonal chemistry and process aims to investigate the following three hypothesis: (i) The in situ encapsulation of enzymes in the inner cavity results in a high encapsulation efficiency since all the molecules dissolved in the aqueous nanodroplets are supposed to be covered by the silica shell. (ii) The core–shell structure protects the enzymes from degradation by external proteolytic attack. (iii) Substrates and products of enzymatic reactions can freely diffuse in and out from the AMSNs due to the semipermeable silica shell.

HRP or GOD was first dissolved in sodium phosphate buffer (pH 7.4), which was converted to aqueous nanodroplets after emulsification, followed by direct encapsulation of the enzymes in the aqueous core of AMSNs after the silica shell formation. The resulting AMSNs hosting the enzymes were denoted as HRP@AMSNs or GOD@AMSNs, respectively. TEM and SEM images show much smaller pore sizes of the silica shell (Figure 3E and Figure S3) in comparison to the dimensions of HRP and GOD macromolecules (HRP: 6.2×4.3×1.2 nm, GOD: 7.7×6.0×5.2 nm).[20] Therefore, the leakage of encapsulated enzymes can be prevented. To quantify the encapsulation efficiency, we centrifuged consecutively the supernatants of the AMSN dispersions in order to achieve their maximum separation from non-encapsulated enzymes remaining in the medium. After five centrifugations, proteins from the pellets and supernatants were quantified, showing high encapsulation efficiency for both HRP and GOD, with 88 % and 78 % of the respective enzymes detected in the AMSNs-containing pellets (Figure 5B), representing ca. 843 HRP and 205 GOD molecules encapsulated per AMSN, respectively. In compar-

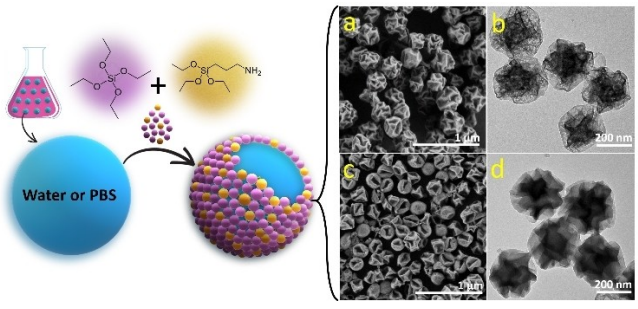

Figure 4. Schematic illustration, and SEM and TEM images of AMSNs synthesized through an interface-confined silica co-condensation process, using ultrapure water (pH 7.0, a), b) or PBS (pH 7.4, (c), (d)) as the water phase of an inverse miniemulsion. A combination of APTES and TMOS (molar ratio of APTES:TMOS = 16 %:84 %) was used as the silica source.

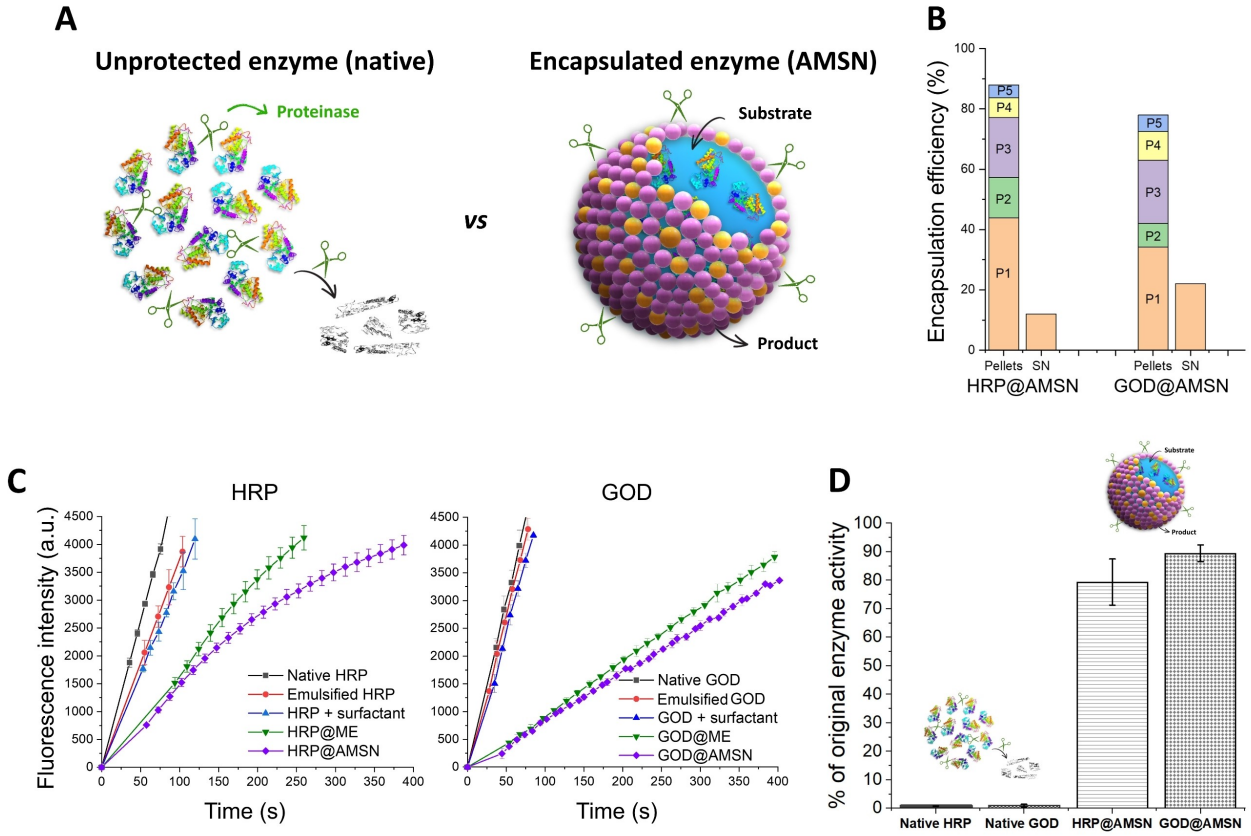

Figure 5. A) Schematic illustration of the in situ encapsulation of enzymes inside AMSNs and the resulting protection against proteolysis. B) Encapsulation efficiency of enzymes in AMSNs. Supernatants of AMSNs dispersions were centrifuged consecutively in order to achieve a maximum separation from non-encapsulated enzymes remaining in the medium. After five centrifugations, enzymes from the pellets and supernatants were quantified by BCA assay. P1-5 represent the pellets after consecutive centrifugation steps. SN represents the remaining supernatant. C) Comparative activities of enzymes in their native form and after submission to different AMSNs synthesis steps or reagents. Emulsified = microfluidization; surfactant = PGPR and Lutensol AT50; enzyme@ME = samples emulsified by the miniemulsion process; enzyme@AMSNs = nanoencapsulated enzymes as final products. D) Native and AMSN-encapsulated enzyme activity after incubation with proteinase K for 24 h. Results were compared to the activity of native enzymes incubated without proteinase K, which represents 100%. Results from three independent experiments are presented as mean ± SD.

ison, centrifugation did not precipitate free enzymes (Figure S12). Dynamic light scattering (DLS) data show that the residual enzymes detected in the supernatants are actually from the small AMSNs that cannot be completely purified by centrifugation (Figure S13); therefore, corroborating the idea that all the molecules dissolved in the aqueous nanodroplets are encapsulated by the silica shell.

To prove the bioorthogonal encapsulation, we investigated how the conditions of the encapsulation process (organic solvent, surfactants, and emulsification) or the diffusion barrier created by the surfactants and silica layers influence the enzyme activity. We compared the activities of native enzymes to (i) enzymes emulsified by microfluidization, (ii) solubilized enzymes incubated with the two surfactants (PGPR and Lutensol AT50) that are used for the nanocapsule preparation, (iii) enzymes emulsified by the miniemulsion process (i.e., the same used for preparing AMSNs), but without the silica shell formation step (noted as enzyme@ME), and (iv) enzyme@AMSNs, which are the nanoencapsulated enzymes as final products. Figure 5C shows that after emulsification or incubation with surfactants, enzymes are only slightly less active than in their native form, suggesting the inertness of these factors against the biomolecules. However, both enzymes@ME and enzyme@AMSNs show slower reaction kinetics, which suggests a confinement effect that hinders the diffusion of substrates and products between the two separate phases. The enzymes@ME are covered with a double surfactant (PGPR and Lutensol AT50) layer, while AMSN-encapsulated enzymes present an additional silica shell. Therefore, both layers likely slow down the diffusion process and consequently reduce the overall reaction speed.

Ideally, the core–shell structure of AMSNs should protect the enzymes against external proteolytic degradation, while the porous shell still allows the free diffusion of low molecular weight substrates and products of the enzymatic reaction. As shown in Figure 5D, native HRP and GOD completely lost their catalytic capacity after incubation with proteinase K for 24 h. In contrast, the activities of encapsulated enzymes were largely preserved (over 80%

and 90 % for HRP and GOD, respectively) upon proteinase K attack due to the protection conferred by the silica shell.

Herein, we further prove the conceptual value of enzyme-encapsulated AMSNs as synthetic organelles. The efficient encapsulation of enzymes in AMSNs provides a new approach for constructing robust synthetic nano-organelles that can be integrated into micrometer-sized compartments to create hierarchical cell-like systems. To demonstrate this, AMSNs nanoreactors carrying HRP and GOD were encapsulated in micrometer-sized block polymer (poly(butadiene)-*b*-poly(ethylene oxide)) giant unilamellar vesicles (pGUVs) to simulate the nano-in-micro structure of eukaryotic cells (Figure 6A). Encapsulation was achieved by a microfluidic assembly method. The combination of stable dispersions of silica nanoreactors with microfluidics resulted in high encapsulation efficiency in polymer vesicles. The multicompartment system consisted of monodisperse polymer vesicles (ca. 62 μm in diameter from microscopy images), each containing approximately 0.09 % (weight) of HRP@AMSNs and 0.09 % of GOD@AMSNs. The microreactors were capable of processing a model substrate (Amplex Red) through its oxidation to a fluorescent product (resorufin) (Figure 6B). The reaction begins with the addition of Amplex Red in DMSO to the external aqueous medium. The Amplex Red diffuses and is taken up by the microreactors, triggering a two-step cascade reaction determined by the AMSN nanoreactors. The maximum fluorescence intensity measured by confocal laser scanning microscopy (CLSM) was reached after approximately 80 seconds (Figure 6C). When substrate (Amplex red) was supplied at a higher concentration of 150 μM, the reaction can be maintained for more than 20 min (Figure S14).

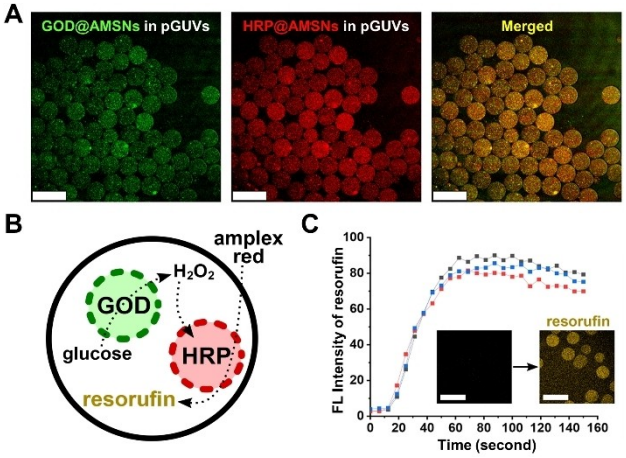

Figure 6. Cell-like multi-compartmentalized microreactors composed of AMSN-nanoreactors. A) Confocal laser scanning microscopy (CLSM) images showing the separated and merged emission of nanoreactors containing HRP and GOD. The nanoreactors were labelled with CY5 and FITC, respectively. B) Schematics of the HRP/GOD microreactor illustrating the oxidation of Amplex Red to form the fluorescent resorufin product. C) Conversion of Amplex Red obtained by image analysis of CLSM data. The inset shows micrographs at time zero and 150 s (end point). The initial concentration of glucose and Amplex Red were 30 mM and 2.44 μM, respectively. Scale bar 100 μm.

Additionally, enzymes encapsulated in silica nanocapsules reached the maximum fluorescence intensity faster than free in-bulk enzymes, which can be attributed to the protection of silica shell that prevents undesired interactions of enzyme with the polymersomes as well as the higher enzyme concentration in nanocapsules that leads to fast reaction kinetics (Figure S15).

Conclusion

We developed a universal approach for the straightforward synthesis of aqueous-core semipermeable silica nanocapsules through an interface-confined sol-gel process. This in situ encapsulation approach provides quantitative encapsulation of enzymes with almost 100 % loading efficiency that overcomes the conventionally uncontrolled loading by adsorption to the particles. The semi-permeable silica shell keeps enzymes enclosed and protected, while allowing the necessary mass exchange with the environment for the enzymatic reactions. We successfully used the enzyme-carrying nanocapsules as nano-organelles in a cell-like system, showing that individually encapsulated enzymes can perform cascade reactions in a multi-compartmentalized environment, mimicking the structure and reactions of eukaryotic cells. Moreover, the internal space of nanocapsules provides a confined environment for efficient cascade reactions of enzyme pairs by increasing the local concentration of intermediate products, which is a valuable feature for further regulating the multi-step reactions and mimicking complex biological processes in the cells.

Acknowledgements

J.P.G. thanks to CAPES (PDSE international PhD exchange program, process number 88881.188473/2018-01) for the fellowship. This work is part of the research conducted within the Max Planck Consortium for Synthetic Biology (MaxSynBio) jointly funded by the Federal Ministry of Education and Research of Germany (BMBF) and the Max Planck Society. Open Access funding enabled and organized by Projekt DEAL.

Conflict of Interest

The authors declare no conflict of interest.

Data Availability Statement

The data that support the findings of this study are available from the corresponding author upon reasonable request.

Keywords: Artificial Cell · Enzyme Encapsulation · Hollow Silica Nanoparticle · Nanoreactor · Polymer Vesicle

[1] a) J. Flechsler, T. Heimerl, H. Huber, R. Rachel, I. A. Berg, *Proc. Natl. Acad. Sci. USA* **2021**, *118*, e2022114118; b) H. C. Kistler, K. Broz, *Front. Microbiol.* **2015**, *6*, 68; c) L. Meldi, J. H. Brickner, *Trends Cell Biol.* **2011**, *21*, 701–708.

[2] a) W. Sato, T. Zajkowski, F. Moser, K. P. Adamala, *Wiley Interdiscip. Rev. Nanomed. Nanobiotechnol.* **2022**, *14*, e1761; b) C. Guindani, S. L. Da, S. Cao, T. Ivanov, K. Landfester, *Angew. Chem. Int. Ed.* **2022**, *61*, e202110855; *Angew. Chem.* **2022**, *134*, e202110855; c) Y. Elani, *Angew. Chem. Int. Ed.* **2021**, *60*, 5602–5611; *Angew. Chem.* **2021**, *133*, 5662–5671; d) A. Belluati, I. Craciun, C. E. Meyer, S. Rigo, C. G. Palivan, *Curr. Opin. Biotechnol.* **2019**, *60*, 53–62; e) K. Göpfrich, I. Platzman, J. P. Spatz, *Trends Biotechnol.* **2018**, *36*, 938–951.

[3] a) F. Cuomo, A. Ceglie, A. De Leonardis, F. Lopez, *Catalysts* **2019**, *9*, 1; b) T. Nishimura, K. Akiyoshi, *Adv. Sci.* **2018**, *5*, 1800801; c) J. Gaitzsch, X. Huang, B. Voit, *Chem. Rev.* **2016**, *116*, 1053–1093.

[4] a) M. Allaw, M. L. Manca, J. C. Gómez-Fernández, J. L. Pedraz, M. C. Terencio, O. D. Sales, A. Nacher, M. Manconi, *Nanomedicine* **2021**, *16*, 2363–2376; b) B. Haller, K. Göpfrich, M. Schröter, J. W. Janiesch, I. Platzman, J. P. Spatz, *Lab Chip* **2018**, *18*, 2665–2674; c) H. Wang, Z. Zhao, Y. Liu, C. Shao, F. Bian, Y. Zhao, *Sci. Adv.* **2018**, *4*, t2816; d) N. Martin, J. P. Douliez, Y. Qiao, R. Booth, M. Li, S. Mann, *Nat. Commun.* **2018**, *9*, 3652; e) H. Tan, S. Guo, N. D. Dinh, R. Luo, L. Jin, C. H. Chen, *Nat. Commun.* **2017**, *8*, 663; f) O. Kreft, M. Prevot, H. Möhwald, G. B. Sukhorukov, *Angew. Chem. Int. Ed.* **2007**, *46*, 5605–5608; *Angew. Chem.* **2007**, *119*, 5702–5705.

[5] a) S. Jiang, M. Mottola, S. Han, R. Thiramanas, R. Graf, I. Lieberwirth, V. Mailänder, D. Crespy, K. Landfester, *Part. Part. Syst. Charact.* **2020**, *37*, 1900484; b) Y. Zhang, B. Y. Hsu, C. Ren, X. Li, J. Wang, *Chem. Soc. Rev.* **2015**, *44*, 315–335; c) S. Jiang, D. Prozeller, J. Pereira, J. Simon, S. Han, S. Wirsching, M. Fichter, M. Mottola, I. Lieberwirth, S. Morsbach, V. Mailänder, S. Gehring, D. Crespy, K. Landfester, *Nanoscale* **2020**, *12*, 2626–2637.

[6] a) Y. Zhang, B. Y. Hsu, C. Ren, X. Li, J. Wang, *Chem. Soc. Rev.* **2015**, *44*, 315–335; b) L. Betancor, H. R. Luckarift, *Trends Biotechnol.* **2008**, *26*, 566–572; c) H. P. Erickson, *Biol. Proced. Online* **2009**, *11*, 32–51; d) Z. Teng, X. Su, Y. Zheng, J. Sun, G. Chen, C. Tian, J. Wang, H. Li, Y. Zhao, G. Lu, *Chem. Mater.* **2013**, *25*, 98–105.

[7] a) J. Liu, T. Liu, J. Pan, S. Liu, G. Lu, *Annu. Rev. Chem. Biomol. Eng.* **2018**, *9*, 389–411; b) A. Khanal, Y. Inoue, M. Yada, K. Nakashima, *J. Am. Chem. Soc.* **2007**, *129*, 1534–1535; c) K. An, T. Hyeon, *Nano Today* **2009**, *4*, 359–373; d) F. Tang, L. Li, D. Chen, *Adv. Mater.* **2012**, *24*, 1504–1534.

[8] a) Y. Zhang, B. Y. Hsu, C. Ren, X. Li, J. Wang, *Chem. Soc. Rev.* **2015**, *44*, 315–335; b) Y. Chen, H. R. Chen, J. L. Shi, *Acc. Chem. Res.* **2014**, *47*, 125–137; c) J. Liu, Q. Yang, L. Zhang, H. Yang, J. Gao, C. Li, *Chem. Mater.* **2008**, *20*, 4275–4286; d) H. Tian, J. Zhao, X. Wang, L. Wang, H. Liu, G. Wang, J. Huang, J. Liu, G. Lu, *Natl. Sci. Rev.* **2020**, *7*, 1647–1655.

[9] C. Zhang, K. Yan, C. Hu, Y. Zhao, Z. Chen, X. Zhu, M. Möller, *J. Mater. Chem. B* **2015**, *3*, 1261–1267.

[10] Y. Zhang, B. Y. Hsu, C. Ren, X. Li, J. Wang, *Chem. Soc. Rev.* **2015**, *44*, 315–335.

[11] a) F. P. Chang, Y. Hung, J. H. Chang, C. H. Lin, C. Y. Mou, *ACS Appl. Mater. Interfaces* **2014**, *6*, 6883–6890; b) F. P. Chang, Y. P. Chen, C. Y. Mou, *Small* **2014**, *10*, 4785–4795; c) Z. Chen, L. Yang, Y. Yan, D. Qi, Z. Cao, *Colloid Polym. Sci.* **2014**, *292*, 1585–1597; d) Z. Cao, L. Dong, L. Li, Y. Shang, D. Qi, Q. Lv, G. Shan, U. Ziener, K. Landfester, *Langmuir* **2012**, *28*, 7023–7032.

[12] C. H. Lin, J. H. Chang, Y. Q. Yeh, S. H. Wu, Y. H. Liu, C. Y. Mou, *Nanoscale* **2015**, *7*, 9614–9626.

[13] a) N. Chopra, V. G. Gavalas, L. G. Bachas, B. J. Hinds, L. G. Bachas, *Anal. Lett.* **2007**, *40*, 2067–2096; b) M. H. Mashhadizadeh, *J. Nanomed. Nanotechnol.* **2012**, *3*, 1000139; c) J. Kim, N. Korkmaz, C. H. Nam, *Interdiscip. Bio Cent.* **2012**, *4*, 1.

[14] F. J. Karol, C. Wu, W. T. Reichle, N. J. Maraschin, *J. Catal.* **1979**, *60*, 68–76.

[15] a) J. W. Carvalho, F. A. Carvalho, T. Batista, P. S. Santiago, M. Tabak, *Colloids Surf. B* **2014**, *118*, 14–24; b) P. S. Santiago, L. M. Moreira, E. V. de Almeida, M. Tabak, *Biochim. Biophys. Acta Gen. Subj.* **2007**, *1770*, 506–517.

[16] R. M. Ottenbrite, J. S. Wall, J. A. Siddiqui, *J. Am. Ceram. Soc.* **2000**, *83*, 3214–3215.

[17] L. Chu, M. I. Tejedor-Tejedor, M. A. Anderson, *Microporous Mater.* **1997**, *8*, 207–213.

[18] I. A. Rahman, M. Jafarzadeh, C. S. Sipaut, *Ceram. Int.* **2009**, *35*, 1883–1888.

[19] U. Schubert, *The Sol-Gel Handbook*, Wiley-VCH, Weinheim, **2015**.

[20] a) C. C. Chen, J. S. Do, Y. Gu, *Sensors* **2009**, *9*, 4635–4648; b) S. Libertino, V. Aiello, A. Scandurra, M. Renis, F. Sinatra, *Sensors* **2008**, *8*, 5637–5648.

Manuscript received: November 17, 2022
Accepted manuscript online: December 14, 2022
Version of record online: February 6, 2023